Utilizing SiGe HBT Power Detectors for Sensing Single-Event Transients in RF Circuits

Adrian Ildefonso, Christopher T. Coen, Zachary E. Fleetwood, George N. Tzintzarov, Mason T. Wachter, Ani Khachatrian, Dale McMorrow, Jeffrey H. Warner, Pauline Paki, and John D. Cressler

***Abstract*— This paper demonstrates the use of an RF power detector to sense the occurrence of single-event transients (SETs) in RF circuits and systems. The detector was connected to a low-noise amplifier (LNA), and the relationship between the detector output and the LNA transients was investigated via two-photon absorption, pulsed-laser testing, together with mixed-mode TCAD simulations. The response of the detector shows a strong correlation with the RF power of the generated SET. An analytical expression for the detector output is derived and utilized to fit the data. The effects of parameters affecting circuit performance on the detector response to SETs are explored using calibrated TCAD mixed-mode simulations, and design tradeoffs are presented. Finally, a solution to distinguish between transients generated in the detector from those generated in the circuit being monitored is proposed and verified in simulation. The use of detectors to monitor SETs in RF systems could lead to judicious deployment of detection-driven SET mitigation techniques.**

***Index Terms*— RF systems, silicon–germanium heterojunction bipolar transistors (SiGe HBTs), single-event transients (SETs), two-photon absorption (TPA) laser testing.**

I. Introduction

ORBITAL radiation environments can strongly limit the performance and reliability of spacecraft payloads. Mitigation techniques are typically put in place to prolong the lifetime of these systems. Throughout the duration of a mission, however, single-event transients (SETs) generated by energized particles can still penetrate spacecraft shielding, potentially disrupting the proper operation of circuits. The circuits receiving messages from a ground station are particularly sensitive to these events, since they carry the weakest signals due to long transmission distances and atmospheric attenuation. Therefore, detecting single-event effects is of importance for the proper operation of these systems.

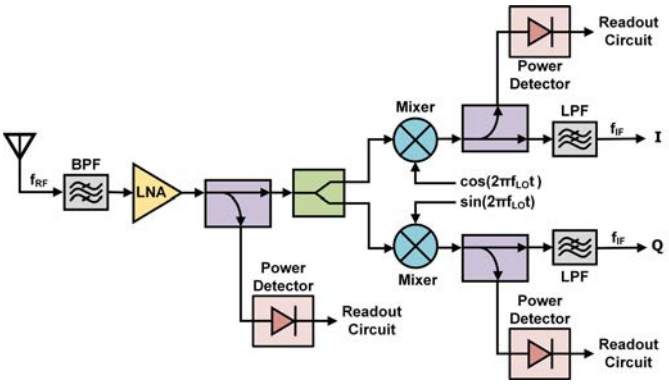

Fig. 1. Simplified schematic of a typical direct-conversion receiver showing the bandpass filter (BPF), LNA, mixers, and LPFs. Directional couplers are used in multiple nodes to sample a portion of the signal and feed it to power detectors for sensing SETs.

The previous work has shown that it is possible to design analog circuits to sense SETs by monitoring changes in voltage or currents in a circuit [1], [2]. In addition, several methods for transient detection in the digital domain have been proposed [3]. However, no methods for sensing SETs in RF systems were found in the literature.

RF power detectors are typically used in a variety of applications, including millimeter-wave radiometry [4], envelope detection [5], and built-in-self-testing of RF systems [6], [7]. Silicon–germanium heterojunction bipolar transistors (SiGe HBTs) are excellent candidates to fabricate detectors for space applications, since their performance improves at low temperatures and they exhibit a built-in tolerance to total ionizing dose (TID) up to several Mrad(SiO_2) [8].

This paper proposes the use of RF power detectors to sense the occurrence of an SET in RF communications systems. By sampling a small fraction of the signal from the main data path into a power detector, information about the signal-to-noise and distortion ratio can be obtained. This information can be used by the digital subsystem to implement detection-driven data correction protocols. The proposed concept is illustrated in Fig. 1, which depicts a simplified schematic of a direct-conversion RF receiver. The RF receiver uses several directional couplers between each stage that direct a small fraction of the main signal to the input of an RF power detector. In this case, the output of each detector would be

Manuscript received July 14, 2017; revised October 3, 2017; accepted October 26, 2017. Date of publication November 13, 2017; date of current version January 17, 2018. This work was supported in part by the Defense Threat Reduction Agency under Contract HDTRA-1-13-C-0058 and in part by the National Science Foundation Graduate Research Fellowship under Grant DGE-1148903.

A. Ildefonso, Z. E. Fleetwood, G. N. Tzintzarov, M. T. Wachter, and J. D. Cressler are with the School of Electrical and Computer Engineering, Georgia Institute of Technology, Atlanta, GA 30332-0250 USA (e-mail: iadrian@gatech.edu; cressler@ece.gatech.edu).

C. T. Coen is with the Advanced Concepts Laboratory, Georgia Tech Research Institute, Atlanta, GA 30332 USA.

A. Khachatrian is with Sotera Defense, Annapolis Junction, MD 20701 USA.

D. McMorrow and J. H. Warner are with the Naval Research Laboratory, Washington, DC 20052 USA.

P. Paki is with the Defense Threat Reduction Agency, Fort Belvoir, MD 22060 USA.

Color versions of one or more of the figures in this paper are available online at http://ieeexplore.ieee.org.

Digital Object Identifier 10.1109/TNS.2017.2772924

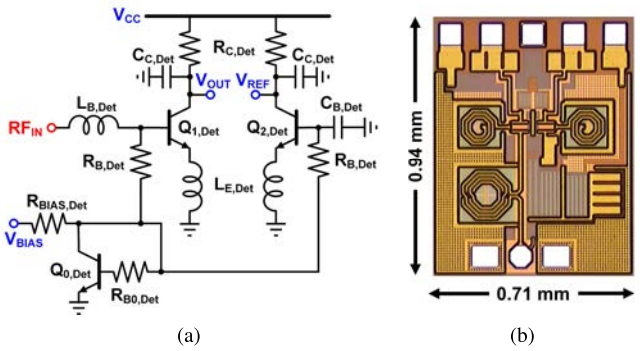

Fig. 2. (a) Schematic and (b) photomicrograph of the designed and fabricated RF power detector measuring 0.71 mm × 0.94 mm including bondpads.

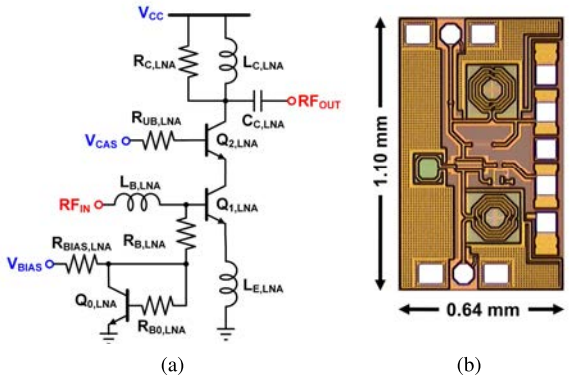

Fig. 3. (a) Schematic and (b) photomicrograph of the designed and fabricated LNA measuring 1.1 mm × 0.64 mm including bondpads.

connected to an analog-to-digital converter that would monitor changes in the output voltage of the detector. The use of several detectors at different stages in the receiver allows to determine the block in which the SET originated.

This investigation has three major goals: 1) demonstrate, for the first time, the use of RF power detectors to detect SETs originated in a low-noise amplifier (LNA); 2) obtain an analytical expression for the detector response to SETs; and 3) establish best design practices for optimizing power detectors for sensing SETs. The results of this work show through experimental data and simulations that power detectors can be used as a system-level SET detection tool to provide diagnostic information for SET mitigation.

II. Circuit Description and Operation

A. Circuit Design and Fabrication

The presented circuits were designed using GlobalFoundries' 8HP platform, a 130-nm SiGe BiCMOS process that features SiGe HBTs with f_T/f_{MAX} of 200/285 GHz. The power detector consists of an inductively degenerated common-emitter SiGe HBT, $Q_{1,\mathrm{Det}}$, with a relatively large load resistor ($R_{C,Det} = 1$ kΩ) and an output shunt capacitor to filter out the fundamental tone of the input signal. An inductor on the base was used to compensate for the input capacitance and improve the input matching at the frequencies of interest. A schematic and a photomicrograph of the fabricated detector are shown in Fig. 2. A reference path, which uses an identical SiGe HBT with a shunt capacitor at the RF input, is also included in the circuit. Typically, the differential output voltage is monitored (i.e., $V_{\mathrm{REF}} - V_{\mathrm{OUT}}$). This compensates for drift in the zero-power output voltage due to temperature swings or any damage resulting from TID.

In this paper, the RF circuit being monitored by the detector consists of an LNA to serve as a proof of concept. A schematic of the LNA and a photomicrograph are shown in Fig. 3. The LNA was implemented using a cascode topology and was designed for simultaneous power and noise matching [9]. This topology was chosen, because it provides higher gain and improved isolation between the input and output nodes when compared with a single common-emitter configuration, and is commonly used at these frequencies. The core is biased at a current density of $J_C = 0.93$ mA/μm^2, which results in the minimum achievable noise figure ($\mathrm{NF_{min}}$). To simplify experimental testing, the LNA and the detector were integrated on-chip, and the output of the LNA was directly connected to the input of the power detector using a 50-Ω on-chip microstrip line (i.e., no coupler was used in this experiment).

B. Theory of Circuit Operation

The following discussion presents a theoretical analysis of the operation of an RF power detector. The analysis can then be expanded to demonstrate the goal of SET detection. It is assumed that all devices are operating in the forward-active region and that there are no dc offsets between the output and reference paths when no RF input is applied.

For a constant-amplitude, continuous-wave (CW) input signal at a single frequency, the change in the differential output voltage of the detector can be expressed by [10]

$$\Delta V_{out} = R_{C,\mathrm{Det}} I_S e^{V_{\mathrm{BE}}/V_T} (e^{V_{\mathrm{RF}}\cos(2\pi f_{\mathrm{RF}} t)/V_T} - 1) \quad (1)$$

$$= R_{C,\mathrm{Det}} I_C (e^{V_{\mathrm{RF}}\cos(2\pi f_{\mathrm{RF}} t)/V_T} - 1) \quad (2)$$

where $R_{C,\mathrm{Det}}$ is the load resistor, I_S is the reverse saturation current, V_{BE} is the dc bias voltage of the common-emitter device, $V_T = \mathrm{kT}/q$ is the thermal voltage, V_{RF} is the amplitude of the input signal, and f_{RF} is the frequency of the sinusoidal wave.

By using the Taylor series expansion, truncated to the first three terms, the exponential can be approximated by

$$e^{V_{\mathrm{RF}}\cos(2\pi f_{\mathrm{RF}} t)/V_T} \approx 1 + \frac{V_{\mathrm{RF}}\cos(2\pi f_{\mathrm{RF}} t)}{V_T} + \frac{V_{\mathrm{RF}}^2 \cos^2(2\pi f_{\mathrm{RF}} t)}{2V_T^2}.$$

With this approximation, the mean value can be calculated

$$f_{\mathrm{RF}} \int_0^{1/f_{\mathrm{RF}}} e^{V_{\mathrm{RF}}\cos(2\pi f_{\mathrm{RF}} t)/V_T} dt \approx 1 + \frac{V_{\mathrm{RF}}^2}{4V_T^2}. \quad (3)$$

Substituting this result into (2), the following relation is obtained:

$$\Delta V_{\mathrm{out}} = R_{C,\mathrm{Det}} I_C \frac{V_{\mathrm{RF}}^2}{4V_T^2}. \quad (4)$$

This response shows a quadratic dependence of the output voltage on the amplitude of the input sinusoid, which, when

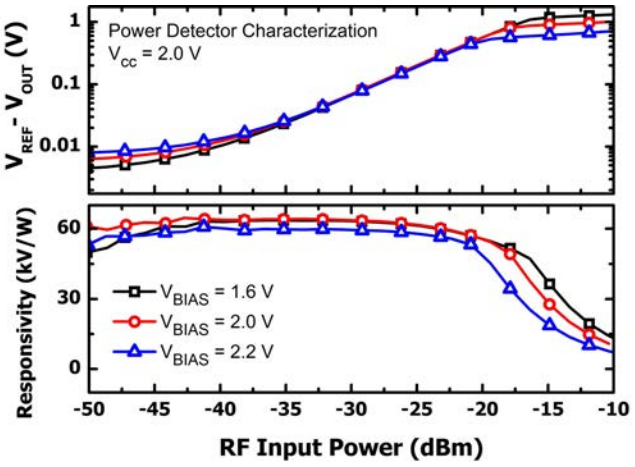

Fig. 4. Measured differential output voltage ($V_{\mathrm{REF}} - V_{\mathrm{OUT}}$) of the SiGe HBT power detector versus RF input power.

converted into input power, translates into a linear relationship. The change in output voltage as a function of input power is a common performance metric for power detectors, also known as responsivity $\Re$, and is defined by

$$\Re = \frac{\Delta V_{\mathrm{out}}}{P_{\mathrm{in}}} = \alpha R_{C,\mathrm{Det}} I_C \tag{5}$$

where α has units of W^{-1} and is a constant that relates the input voltage to input power while considering the effects of impedance mismatch [10]. The measured ΔV_{OUT} of the presented power detector as a function of input power, as well as its responsivity, is shown in Fig. 4, for multiple bias voltages. The plot shows a linear dependence of the change in output voltage with respect to change in input power. Deviations from the linear operation at low input powers are due to small dc offsets between the output and reference paths, while deviations at high input powers are due to the SiGe HBT on the output path entering the saturation region of operation.

Although the preceding theory was applied to a CW input, the procedure follows from the analysis of the detector circuit. Therefore, a similar analysis can be used to obtain an expression for the change in output voltage due to SETs by starting with the same basic relation

$$\Delta V_{\mathrm{out,SET}} = R_{C,\mathrm{Det}} I_C (e^{V_{\mathrm{SET}}(t)/V_T} - 1) \tag{6}$$

where $V_{\mathrm{SET}}(t)$ is the SET signal in the time domain. Since this function can vary depending on the part of the circuit that is struck by a heavy ion, the derivation of a universal expression is not possible. However, the expression for the change in output voltage when transients are generated in the presented LNA has been derived in Section V.

III. Experimental Setup

Laser-induced transients on the RF circuits were measured at the U.S. Naval Research Laboratory using through-wafer two-photon absorption (TPA) [11]. TPA carrier injection allows for time-resolved, position-dependent 3-D measurements of SETs. The system features 150-fs, 1260-nm wavelength optical pulses at a repetition rate of 1 kHz with a full-width-at-half-maximum (FWHM) focused spot size of approximately 1 μm.

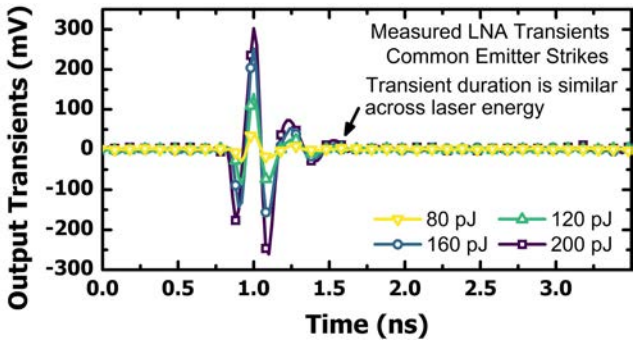

Fig. 5. Output transients in the time domain generated by striking the common-emitter device of the LNA with multiple laser energies.

Each sample was attached and wire-bonded to a custom-designed, high-speed printed circuit board that exposes the backside of the die for irradiation. For this experiment, one set of boards contained a die with just an LNA attached, while another set of boards contained a die with an integrated LNA and detector. Thus, the results shown for the LNA-only and detector output measurements were taken using a different die, although we note that die-to-die performance variations are generally minimal in SiGe technologies. The board uses coplanar waveguides to deliver the signals from the wire bonds to Southwest Microwave SMA end launch connectors. The induced SETs were captured using a Tektronix DPO71254, which is a 12.5-GHz bandwidth real-time oscilloscope capable of capturing 50 GS/s. All circuits were biased using Keithley 2400 source measure units. For some of the results presented, which are explicitly specified in their appropriate sections, a CW signal was delivered to the input of the LNA using an HP 83712A synthesized CW generator; in all other cases, the input was terminated using 50 Ω through a dc block.

IV. Experimental Results and Discussion

A. LNA Output Transients

The common-emitter and common-base devices of the LNA were struck with the TPA laser, and all the data shown are for emitter-center strikes, except for the 2-D raster scans. Fig. 5 shows the SETs for strikes to the common-emitter device for different laser energies. The data show that the transients exhibit a dampened oscillatory response with a similar time constant for all laser energies. To verify the source of this response, the double-exponential model presented in [12] was implemented in MATLAB and fit to the SETs observed at the collector of a single SiGe HBT device when subjected to the TPA laser. This fit transient was convolved with the impulse response of the output matching network, and the resulting signal was compared with TPA-generated SETs measured at the output of the presented LNA. This comparison, which shows excellent agreement between simulations and measurements, can be observed in Fig. 6. The results from these simulations indicate that, for a narrow-band RF circuit, such as the LNA designed for this paper, any matching networks utilized at the output will shape the SET generated at the device level,

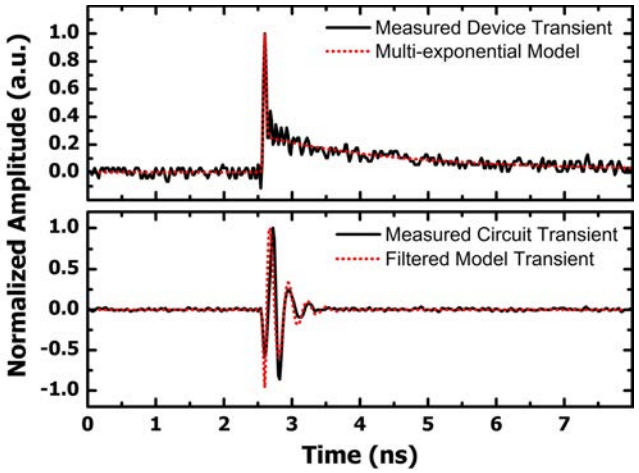

Fig. 6. Top: normalized amplitudes of measured SiGe HBT collector transients and double-exponential model. Bottom: measured LNA output transients compared with device transients filtered with a narrow BPF.

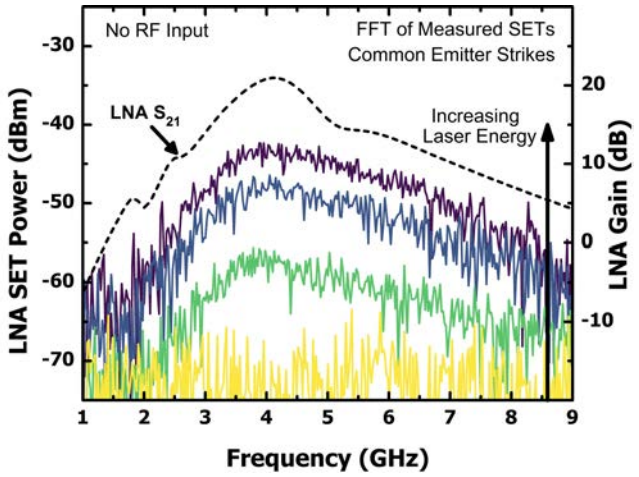

Fig. 7. Power spectra of the measured LNA output transients as a function of frequency for multiple laser energies.

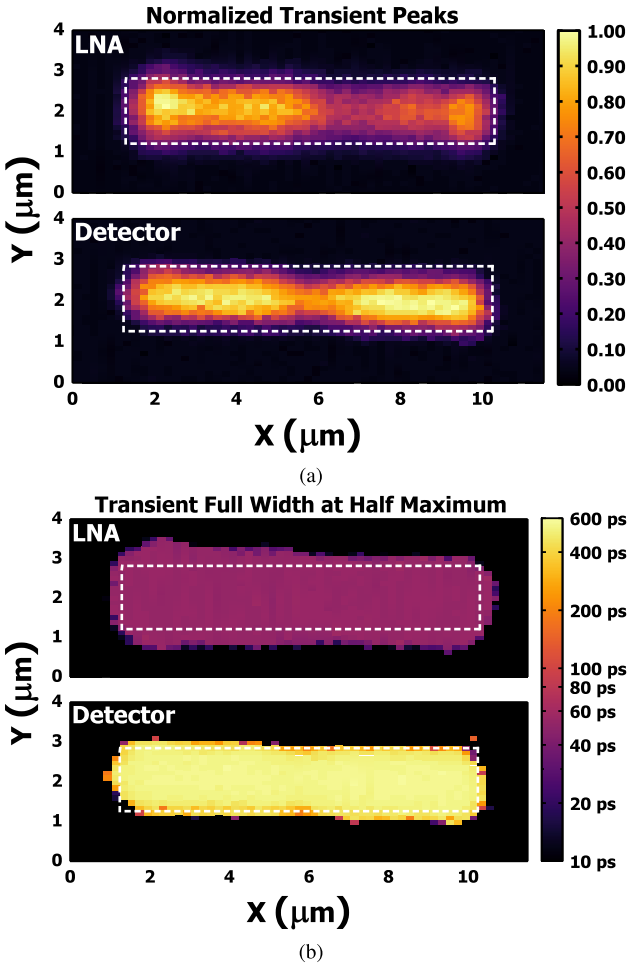

Fig. 8. 2-D raster scan showing (a) normalized transient peaks and (b) transient FWHM of the common-emitter device in the LNA when the output is taken from the LNA (top) and the power detector (bottom). A laser pulsed energy of 120 pJ was used. The white dashed lines outline the intrinsic region of the device.

by shaping the frequency spectrum of the transient at the output node. Therefore, it can be inferred that the circuit-level SETs for a narrow-band system at these low frequencies will be in the band of interest and cannot be filtered out. To further confirm this statement, the power spectra of representative measured transients were calculated in MATLAB using the fast Fourier transform (FFT) and are shown in Fig. 7. The small-signal gain of the LNA is overlaid in a dashed line for comparison. The data show that an increase in laser pulse energy results in a monotonic increase in SET spectral power within the frequency band of interest. This is a significant result as it confirms two major observations: 1) analog or digital filters cannot be used to attenuate the SETs as they would also attenuate the signals carrying data and 2) power detectors tuned to detect signals in the frequency bands of interest will also detect SETs as they will reside in the same frequency bands after being shaped by matching networks.

B. Power Detector Output Transients

To evaluate the efficacy of utilizing a power detector for sensing SETs generated by strikes on the LNA, two different test boards were employed: one with an LNA and another with an integrated LNA and power detector. TPA transients were captured at the LNA output for one test board and the power detector output for the other board.

First, it is important to verify whether the detector can capture transients generated throughout the entire device and not just the most sensitive area. To accomplish this, the laser energy was fixed at approximately 120 pJ, and the beam was scanned across the device, recording transients at each X–Y position. The SET peaks were then normalized to the maximum recorded amplitude and plotted on 2-D raster scans, which are shown in Fig. 8(a). The data show that the power detector output can cover the entire sensitive area of the device. This is important, because it means that transients generated by off-centered strikes will still be detected. In addition, the FWHM duration for LNA transients and detector transients as a function of position is plotted in Fig. 8(b). The data show that detector transients are considerably longer than LNA transients, making it much easier to design the readout circuitry, since this relaxes the required sampling rate.

It is also of interest to verify how well the detector can track the amplitude of the generated SETs in the LNA. To do this,

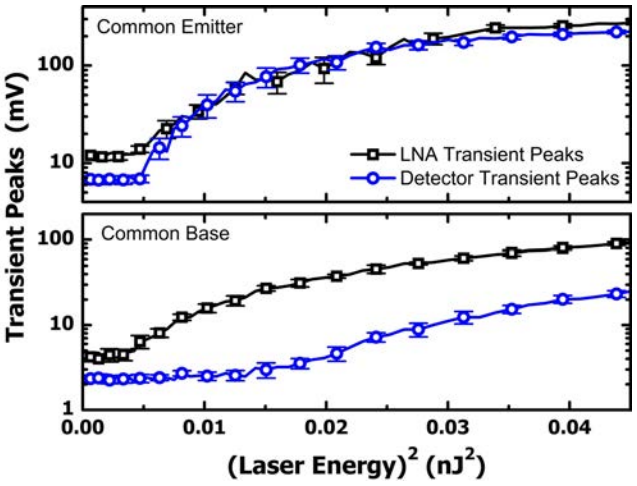

Fig. 9. Magnitude of output transient peaks measured at the LNA output and the detector output as a function of laser energy when each device in the LNA is struck.

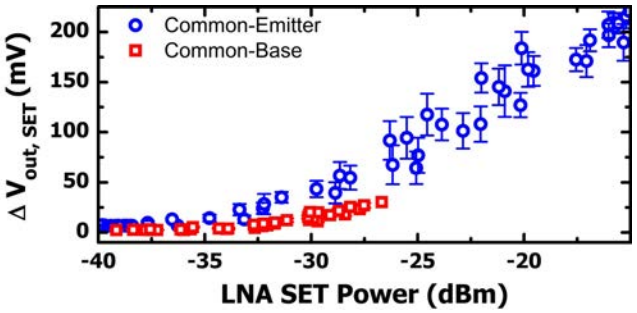

Fig. 10. Magnitude of the detector output transient peaks as a function of LNA output transient power when the devices on the signal path are struck with the laser.

the laser was positioned at the most sensitive area of the common-emitter and common-base devices in the LNA, and the laser pulse energy was swept from 110 to 215 pJ. The transient peaks for the LNA output and the detector output are plotted in Fig. 9, which shows that for common-emitter and common-base strikes above a certain, yet different, energy level, the detector output voltage tracks with the amplitude of the generated transient.

To further explore this apparent detection threshold, the power spectra of the SETs generated at the LNA output were obtained by applying the FFT to the time-domain signals. The detector output peaks for common-emitter and common-base devices were replotted as a function of the calculated LNA SET power in Fig. 10. It can be observed that for SET powers below −35 dBm, the detector is not responsive enough to transients generated by the LNA, regardless of the device struck. This explains the threshold observed in Fig. 9. Note that this threshold is related to the circuit performance shown in Fig. 4, which shows a saturation of the output voltage at a similar input power.

V. SET Modeling and Responsivity Calculation

In Section II-B, the theory of the detector circuit operation was presented, and an expression for changes in output voltage due to a CW input was derived. A similar procedure can be followed to obtain an equivalent relationship for responsivity due to SETs. The main difference is that, for SET detection, the analysis should be performed in terms of peak amplitude, since the output of the detector would be a transient change in voltage, and it is easier to measure peaks than it is to sample the entire transient. In addition, the output capacitor used to filter the fundamental frequency of the input signal must be taken into account, since the transients will be generated in the same frequency band as the signal. The analysis begins with a similar equation for the output voltage, with the addition of a term to account for the charging time of the output capacitor

$$\Delta V_{\text{out,SET}} = R_{C,\text{Det}} I_C \left(e^{\frac{v_{\text{SET}}(t)}{V_T}} - 1 \right) \left(1 - e^{\frac{-t}{\tau_C}} \right) \tag{7}$$

where $\tau_C = R_{C,\text{Det}} C_{C,\text{Det}}$.

The experimental laser results showed that the transients generated at the LNA have a dampened oscillatory response, which can be represented using a functional form for v_{SET} given by

$$v_{\text{SET}}(t) = A e^{-t/\tau} \cos(\omega t) \tag{8}$$

where A is the amplitude of the SET, τ is the decay time constant, and $\omega = 2\pi f_0$ is the fundamental oscillation frequency of the SET, which is determined by the output matching network of the LNA.

Similar to the previously presented derivation of $\Re$, the Taylor series expansion can be used to approximate the exponential in the expression for $\Delta V_{\text{out,SET}}$. In this case, instead of obtaining the average value for the output voltage, the peak value will be used instead. This is achieved by setting $t = 0$ in (8). In addition, since the capacitor voltage cannot change instantaneously, the output voltage will begin to change until the SET amplitude decays to a point where it will no longer force the capacitor voltage to decrease, after which, the capacitor will start recharging and return to its dc voltage. The peak value will be obtained at some time $t = t_0$. The expression for detector output peaks will be given by

$$\Delta V_{\text{out,SET,Pk}} = R_{C,\text{Det}} I_C \left(\frac{A}{V_T} + \frac{A^2}{2V_T^2} \right) \left(1 - e^{\frac{-t_0}{\tau_C}} \right). \tag{9}$$

To write this expression in terms of input power, the rms value for $v_{\text{SET}}(t)$ must be obtained by integrating from $t = 0$ to $t = 5\tau$, where the exponential decays to 0.67% of the initial value. The resulting expression is given by

$$v_{\text{SET,RMS}}(t) = A \sqrt{\frac{1}{20} \left(1 + \frac{1}{1 + \tau^2 \omega^2} \right)}. \tag{10}$$

Using the same α value defined in Section II-B, the peak amplitude can be expressed in terms of the input power P_{in} as

$$A = \sqrt{\frac{40 V_T^2 \alpha P_{\text{in}}}{1 + \frac{1}{1+\tau^2\omega^2}}}. \tag{11}$$

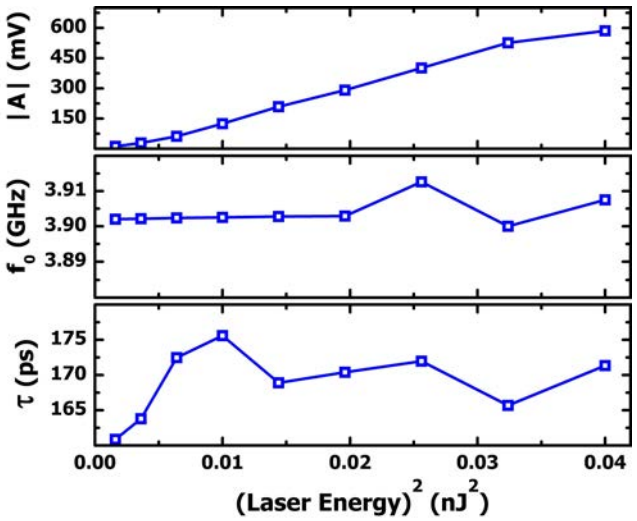

Fig. 11. Parameters used to fit (8) to experimental data as a function of laser energy.

Substituting this expression into (9), the change in output voltage can be expressed in terms of input power by

$$\Delta V_{\text{out,SET,Pk}} = R_{C,\text{Det}} I_C \times \left(\sqrt{\frac{40\alpha P_{\text{in}}}{1+\frac{1}{1+\tau^2\omega^2}}} + \frac{20\alpha P_{\text{in}}}{1+\frac{1}{1+\tau^2\omega^2}} \right) \times \left(1 - e^{\frac{-t_0}{\tau_C}}\right). \quad (12)$$

To verify this expression against the experimental data shown in Fig. 10, appropriate values for τ and ω must first be determined. The experimental data presented in Section IV showed an increase in transient amplitude for increasing laser energy, while the oscillation frequency ω and the decay time constant τ showed no dependence on laser energy. This experimental result allows for the use of a single value for τ and ω, which can be determined from fitting the expression in (8) to individual transients obtained for multiple laser energies. A good fit was achieved for representative transients at all laser energies, and the fitting parameters used are plotted as a function of the laser energy squared in Fig. 11. From this plot, average values for ω and τ can be obtained as $2\pi f_0 = 24.5 \times 10^9$ rad/s and 169 ps, respectively.

The values necessary to fit (12) to experimental data have been obtained. To simplify the discussion, the parameters β and G will be defined as follows:

$$\beta = \frac{1}{1+\tau^2\omega^2} \quad (13)$$

$$G = R_{C,\text{Det}} I_C \quad (14)$$

which simplify (12) to

$$\Delta V_{\text{out,SET,Pk}} = G\left(\sqrt{\frac{40\alpha P_{\text{in}}}{1+\beta}} + \frac{20\alpha P_{\text{in}}}{1+\beta} \right)\left(1 - e^{\frac{-t_0}{\tau_C}}\right). \quad (15)$$

The value for t_0 can be determined by considering a square pulse, with a pulsewidth $= t_0$, as an input to the detector. An expression for rms amplitude can be obtained over a duration of 5τ to be consistent with the rms value obtained for $v_{\text{SET}}(t)$. By equating the rms value of the pulse to the rms value of $v_{\text{SET}}(t)$, it can be determined that $t_0 = \tau$.

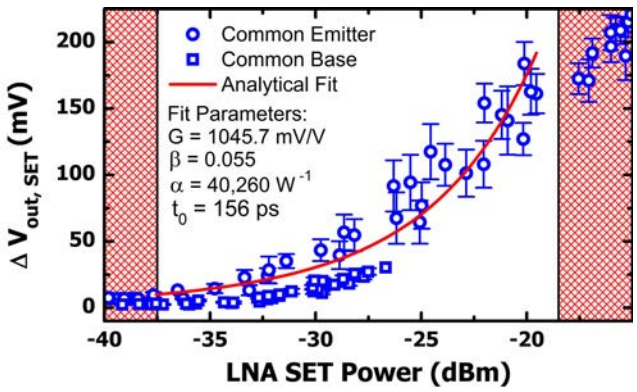

Fig. 12. Comparison of analytical fit to experimental data using (15).

This equation was used to fit the experimental data in Fig. 10. The parameter β was set to 0.055, since it was obtained from experimental fit of LNA transients and is therefore assumed to be fixed. The parameters G, α, and t_0 were varied until the analytical curve fit the measurement data, and the resulting fit is shown in Fig. 12. The shaded red regions designate the range of power levels for which the detector deviates from its linear response for a CW wave input, which will be the ranges for which the analytical model is not valid. The resulting values for G, α, and t_0 were 1045.7 mV/V, 40 260 W^{-1}, and 156 ps, respectively. The obtained values for G and t_0 closely match the circuit gain and the LNA SET time constant, while the obtained value for α falls within the range of values obtained when several samples of the power detector were characterized. The fact that these parameters match circuit performance metrics and LNA SET characteristics proves that the derived equation results in an excellent fit to the experimental data. This analytical equation could be used to calculate the power and amplitude of the generated SET for the measured change in output voltage of the detector.

The main approximation used in the development of this model is the Taylor series expansion in (9). The reader will note that, when the Taylor series is truncated to a second-order polynomial, the mathematical approximation will quickly deviate from the original equation. However, (7) does not take into account device nonlinearities and changes in responsivity due to device saturation. These two approximations have the opposite effects on the resulting expression for the output voltage of the detector (i.e., the truncated series will result in smaller values, while the exclusion of nonlinearities will result in larger values). This results in an acceptable model for the power detector presented in this paper. More terms may be required for a different power detector design.

In addition, the typical detector responsivity equation derived in Section II-B, which shows that the output voltage is proportional to the input power (i.e., a quadratic relation to the input voltage), is only applicable to low RF powers. At higher input powers, the detector output voltage is proportional to the input voltage [13]–[15]. The same concept applies to when the circuit is used for SET detection. Although the model developed in this section can be used to fit the data

with a very good agreement, a more rigorous approach would define a piecewise linear functional relationship. This approach would result in an extended model that would take into account device-level nonlinearities and could cover a greater range of input powers, which is of importance when a detector with high dynamic range is used.

VI. Using Detectors in Communications Systems

A. Detector Design and Optimization

Up to this point, all of the presented results have assumed the performance of the circuit to be constant. From the theory derived in Section II-B, there are three major parameters that can change the responsivity of the circuit: impedance mismatch, contained in the parameter α, bias current I_C, and load resistance $R_{C,\mathrm{Det}}$. Introducing additional impedance mismatch between the detector input and the output of the preceding stage will result in a decreased responsivity. Although introducing some mismatch can result in extended bandwidth in some RF circuits and systems, for a narrow-band system such as the one presented in this paper, this is typically undesirable, and will not be considered in this paper. However, since the goal is to detect transients, the output capacitance is also important, as it will determine the rise time, and by extension the peak, of the detector output. Therefore, the three parameters examined in this section are the load resistance, the load capacitance, and the bias current.

When optimizing detectors for SET measurements, it is important to recall that, contrary to a CW input which produces a dc output, the expected output in this scenario will also be a transient. If the bias current is kept constant, increasing the output resistance and capacitance values will increase the RC time constant at the output of the detector, increasing the rise time and, therefore, reducing the output transient peak. At the same time, for a given input SET, increasing collector resistance will result in a larger peak amplitude at the output. There are two tightly coupled, yet competing factors in this problem. For a given SET voltage input into the detector, a transient current will be generated at the collector of the common-emitter device. Since the output capacitor is meant to filter out the fundamental frequency of the RF signal, then $\tau \ll \tau_C$, and (15) can be rewritten by using a Taylor series expansion truncated to the first two terms as

$$\Delta V_{\mathrm{out,SET,Pk}} = I_C \left(\sqrt{\frac{40\alpha P_{\mathrm{in}}}{1+\beta}} + \frac{20\alpha P_{\mathrm{in}}}{1+\beta} \right) \left(\frac{\tau}{C_{C,\mathrm{Det}}} \right). \quad (16)$$

This shows that the output transients should be independent of load resistance, and inversely proportional to load capacitance.

Since it is not possible to directly change the load resistance and capacitance of the detector without fabricating multiple circuits, the effects of varying these values were verified using Cadence and mixed-mode TCAD simulations. The 2-D SiGe HBT TCAD models have been developed using the Synopsys TCAD suite and calibrated to match the dc and ac characteristics of the Cadence 8HP process design kit compact models. Circuit-level ion-strike simulations were performed on the common-emitter device of the LNA using an linear energy transfer of 10 MeV-cm^2/mg. The output voltage transients were extracted and used as an input to the detector by using a voltage source that takes values from a lookup table. Transient simulations were performed in Cadence to observe the detector response to a transient input.

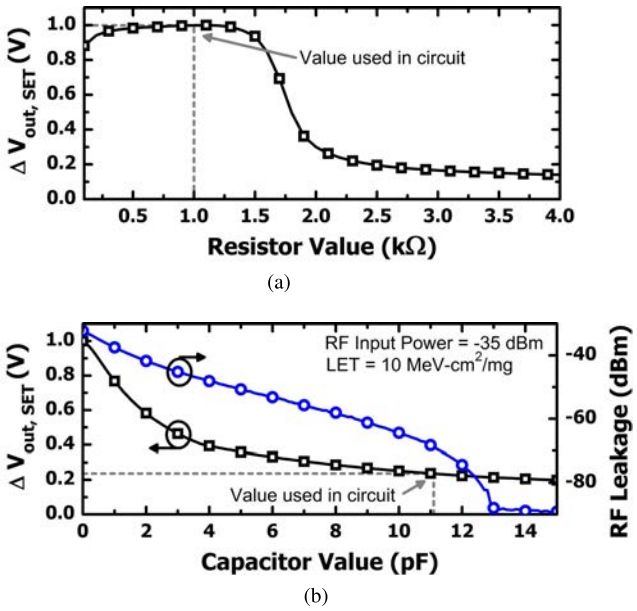

Fig. 13. Simulation of normalized power detector output when the input is a transient produced on the output of the LNA by a heavy-ion strike in the common-emitter device for several (a) resistor and (b) capacitor values. For the capacitor value sweep, the leakage from a CW signal is included when the input RF power is −35 dBm.

The simulation results in Fig. 13(a) show that the detector output transients are independent of load resistance, until the dc collector voltage decreases enough to drive the transistor into saturation, after which the output decreases. These simulation results confirm the expression shown in (16), which assumes that the device is biased in the forward-active region. Note, however, that increasing the load resistance will increase the responsivity of the detector, and may cause the detector response to saturate in the presence of an RF signal (i.e., the signal carrying the modulated data).

As previously mentioned, the output capacitor acts as a low-pass filter (LPF) to suppress the RF signal at the output of the power detector. Since the SET lies in the same frequency band as the RF signal, it will also be suppressed, as shown by (16). Fig. 13(b) shows the simulated normalized output of the detector as a function of increasing output capacitance values. The simulation results show an inverse relationship between the output voltage of the detector due to SETs and capacitance value, which is in agreement with the expression obtained from a circuit analysis. Fig. 13(b) also shows the RF power at the output of the detector as a function of output capacitance value for an RF input power of −35 dBm. The data show that for decreasing capacitor value (which increases the change in output voltage due to SETs), the power of the RF signal detected at the output of the detector increases. Therefore, an inherent tradeoff exists between transient responsivity and suppression of the RF signal at the output.

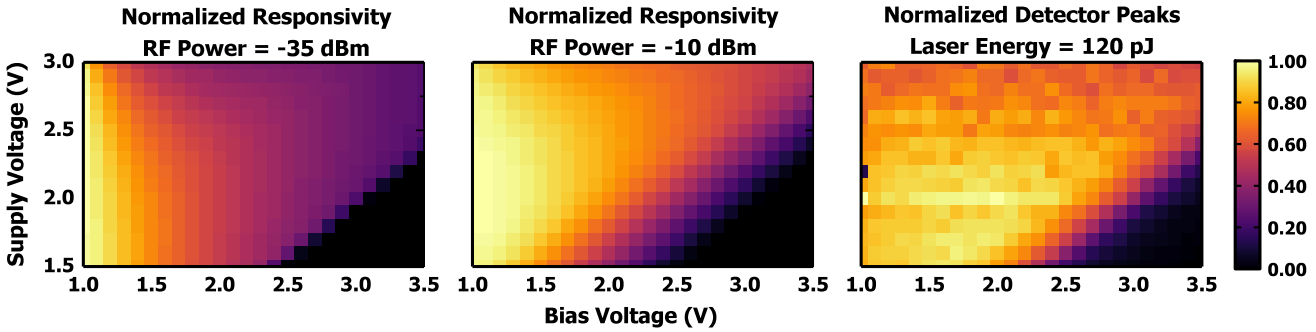

Fig. 14. Comparison of the simulated detector responsivity at an RF input power of −35 and −10 dBm to the measured detector output transient when the laser is focused on the common-emitter device of the LNA. The laser energy used was 120 pJ.

To explore the dependence of circuit performance on bias current, the circuit was simulated by sweeping the bias voltage. For these simulations, the supply voltage was also swept, since a higher supply voltage will result in higher detector linearity with respect to input power. Responsivity values were obtained for the input powers of −35 and −10 dBm, normalized to the peak simulated responsivity, and plotted in Fig. 14 as a function of bias and supply voltage. In addition, TPA results for the same bias and supply voltages were obtained. In these measurements, the laser was focused on the most sensitive part of the common-emitter device of the LNA, and the output of the detector was monitored. The detector output peaks were normalized to the highest measured peak and also plotted in Fig. 14. Both responsivity simulations and TPA measurements show a similar dependence on bias and supply voltage.

The data suggest that designing detectors with higher responsivities will make it easier to detect SETs, an intuitive result. However, a tradeoff exists between detector responsivity and linearity. Increasing responsivity to the highest achievable value to improve SET detection could cause the detector to saturate with the data signal, leading to decreased sensitivity in SET detection. In such a case, the coupling factor of the directional couplers could be reduced to avoid saturation of the detector (i.e., a smaller sample is taken from the main signal). Therefore, having knowledge of the expected signal levels at different points in the RF system is crucial to ensure proper design of detectors.

Note that in addition to the bias current and load resistor, transistor sizing can also affect circuit performance, with smaller devices typically yielding higher responsivities. Further studies should be performed to investigate tradeoffs between transistor sizing and transient responsivity.

B. SET Sensitivity With Input Data

Since the output of the RF circuit or system to be monitored will be fed into the detector via a directional coupler, the RF signal going through the system will also be coupled to the detector input. Therefore, it is pertinent to explore the SET response when an RF input is present. This was achieved by focusing the laser on the common-emitter device of the LNA and applying a CW RF signal to the input of the LNA.

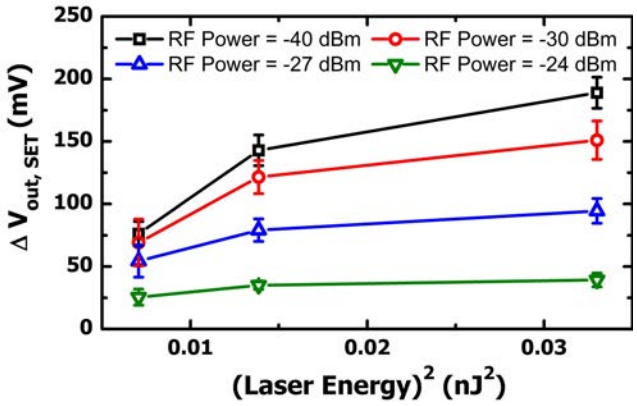

Fig. 15. Measured changes in detector output voltage as a function of laser energy for several values of RF input power.

The output of the power detector was recorded for multiple laser energies and RF input powers. The transient peaks as a function of laser energy are plotted in Fig. 15. The curves show that the change in output voltage increases as a function of laser energy, as expected. For a given laser energy, higher RF input power produces a smaller change in the output voltage. This result suggests that the power detector is capable of indicating the relative power of the generated SET with respect to the power of the RF signal. This is very useful in a scenario where the effects of the SET on the data going through the system are well characterized, since it can allow for the deployment of mitigation techniques that are dependent on the severity of the impact of the generated SET.

Error detection and correction encoding are ubiquitous in communications protocols for most space systems, as they allow for the recovery of corrupted data due to noise, channel interference, and other phenomena that may compromise the proper reception of the transmitted data stream [16]. It is difficult to determine whether these encoding techniques, which are intrinsic to data transmission and processed by digital systems, are sufficient to mitigate SET-induced bit errors resulting from ion strikes on the RF receiver. Although data encoding techniques can significantly reduce bit-error rates at the expense of bandwidth or data rate, to say that they are sufficient to mitigate all SET-induced bit errors requires assumptions of modulation scheme, data encoding scheme,

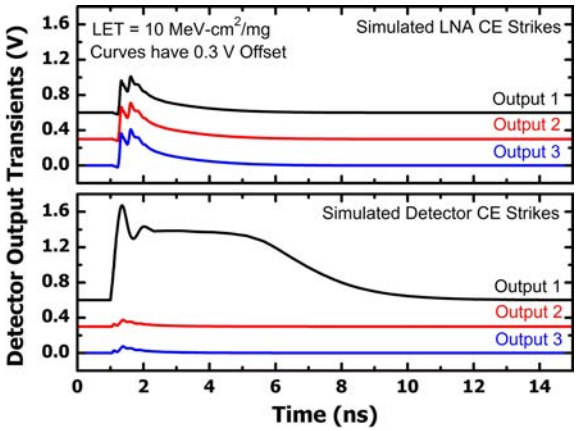

Fig. 16. Simulated detector output transients for heavy-ion strikes on the common-emitter device of the LNA (top) and the common-emitter device of the power detector (bottom). The curves in each plot are offset by 0.3 V for clarity.

carrier frequency, data rate, among others. However, regardless of these parameters, a power detector could be used to provide additional information to the digital system on the occurrence of SETs, which could be used to: 1) confirm that the data correction has been properly achieved (i.e., the affected bit is the one corrected); 2) trigger data retransmission protocols in the event that recovery is not possible; and 3) potentially develop new error-correction methodologies with similar robustness and smaller bandwidth penalties than current approaches.

C. Mitigating Detector Transients

Since the power detector utilizes forward-biased SiGe HBTs, it is also susceptible to SETs. Under normal operation of the detector, the reference path remains unchanged, regardless of whether an SET hits the system of interest or not. Therefore, any transients generated in the reference path would just be ignored by the readout circuit. In addition, a transient generated by a heavy-ion strike on the bias device will propagate through both the output and reference paths, and can be ignored by the readout circuit. However, if a heavy ion passes through the device connected to the detector output, the transient generated could result in a false-positive detection event, since the readout circuitry will not be able to discern between hits to the RF system and hits to the detector itself. A potential mitigation strategy is to implement a concept similar to triple modular redundancy (TMR). However, instead of having three different detectors, one detector with three different output paths and one reference path can be used to reduce power consumption. A majority voting circuit can be implemented in the digital subsystem after the readout circuitry. In this implementation, a three-way power divider would be placed after the directional coupler.

To verify this approach, mixed-mode TCAD simulations were performed. The detector was modified to add two additional output paths. Instead of using a directional coupler, the output capacitor of the LNA was split in three, and connected to each of the detector inputs. Fig. 16 shows the output of the three detector branches when the LNA is struck with a heavy ion compared to when one of the detector paths (Output 1) is struck. For strikes on the LNA, the simulation results show almost identical output transients on all three detector outputs. In contrast, when the heavy ion passes through the detector, only one output, the one connected to the struck device, shows a transient. These results show that SETs on the detector can indeed be mitigated using a pseudo-TMR approach.

VII. Conclusion

This paper proposed the use of an RF power detector to sense the occurrence of SETs in RF circuits and systems. It was shown through TPA experiments that the proposed circuit can be used to detect SETs in the LNA. Furthermore, the output of the detector was shown to yield information about the RF power of the SET, and also detect the relative level of SETs with respect to the input signal. An expression for the detector output voltage as a function of the LNA SET power was derived and resulted in an excellent fit to experimental data. The circuit design tradeoffs were explored using experiments and TCAD simulations, with the main tradeoff being between transient responsivity and suppression of the RF signal carrying data. A solution to distinguish SETs on the RF system of interest and the detector itself that uses a pseudo-TMR approach was demonstrated using mixed-mode TCAD simulations. Utilizing power detectors for sensing SETs can enable the deployment of detection-driven mitigation techniques, as well as the development of more intricate mitigation techniques that depend on the severity of the detected SET.

References

[1] J. M. Espinosa-Duran, J. Velasco-Medina, G. Huertas, R. Velasco, and J. L. Huertas, "Measuring SET effects in a CMOS operational amplifier using a built-in detector," in *Proc. AFRICON*, Sep. 2007, pp. 1–7, doi: 10.1109/AFRCON.2007.4401472.

[2] Z. Zhang, T. Wang, L. Chen, and J. Yang, "A new bulk built-in current sensing circuit for single-event transient detection," in *Proc. IEEE 23rd Can. Conf. Elect. Comput. Eng. (CCECE)*, May 2010, pp. 1–4, doi: 10.1109/CCECE.2010.5575124.

[3] H. Liang, P. Mishra, and K. Wu, "Error correction on-demand: A low power register transfer level concurrent error correction technique," *IEEE Trans. Comput.*, vol. 56, no. 2, pp. 243–252, Feb. 2007.

[4] J. W. May and G. M. Rebeiz, "Design and characterization of *W*-band SiGe RFICs for passive millimeter-wave imaging," *IEEE Trans. Microw. Theory Techn.*, vol. 58, no. 5, pp. 1420–1430, May 2010.

[5] M. Uzunkol, W. Shin, and G. M. Rebeiz, "Design and analysis of a low-power 3–6-Gb/s 55-GHz OOK receiver with high-temperature performance," *IEEE Trans. Microw. Theory Techn.*, vol. 60, no. 10, pp. 3263–3271, Oct. 2012.

[6] R. L. Schmid, P. Song, C. T. Coen, A. C. Ulusoy, and J. D. Cressler, "A *W*-band integrated silicon-germanium loop-back and front-end transmit-receive switch for built-in-self-test," in *IEEE MTT-S Int. Microw. Symp. Dig.*, May 2015, pp. 1–4, doi: 10.1109/MWSYM.2015.7166811.

[7] A. Valdes-Garcia, R. Venkatasubramanian, R. Srinivasan, J. Silva-Martinez, and E. Sanchez-Sinencio, "A CMOS RF RMS detector for built-in testing of wireless transceivers," in *Proc. 23rd IEEE VLSI Test Symp.*, May 2005, pp. 249–254.

[8] J. D. Cressler, "Radiation effects in SiGe technology," *IEEE Trans. Nucl. Sci.*, vol. 60, no. 3, pp. 1992–2014, Jun. 2013.

[9] W.-M. Kuo, Q. L. Q. Liang, J. Cressler, and M. Mitchell, "An X-band SiGe LNA with 1.36 dB mean noise figure for monolithic phased array transmit/receive radar modules," in *Proc. IEEE Radio Freq. Integr. Circuits (RFIC) Symp.*, Jun. 2006, p. 4, doi: 10.1109/RFIC.2006.1651200.

[10] L. Gilreath, V. Jain, and P. Heydari, "Design and analysis of a W-band SiGe direct-detection-based passive imaging receiver," *IEEE J. Solid-State Circuits*, vol. 46, no. 10, pp. 2240–2252, Oct. 2011.

[11] D. McMorrow, W. T. Lotshaw, J. S. Melinger, S. Buchner, and R. L. Pease, "Subbandgap laser-induced single event effects: Carrier generation via two-photon absorption," *IEEE Trans. Nucl. Sci.*, vol. 49, no. 6, pp. 3002–3008, Dec. 2002.

[12] D. A. Black, W. H. Robinson, I. Z. Wilcox, D. B. Limbrick, and J. D. Black, "Modeling of single event transients with dual double-exponential current sources: Implications for logic cell characterization," *IEEE Trans. Nucl. Sci.*, vol. 62, no. 4, pp. 1540–1549, Aug. 2015.

[13] S. Rami, A. Paganini, and W. R. Eisenstadt, "A minimally invasive wide-band mixed-mode detector for mm-wave BIST applications," in *Proc. 60th Electron. Compon. Technol. Conf. (ECTC)*, Jun. 2010, pp. 735–743.

[14] T. Zhang, W. R. Eisenstadt, R. M. Fox, and Q. Yin, "Bipolar microwave RMS power detectors," *IEEE J. Solid-State Circuits*, vol. 41, no. 9, pp. 2188–2192, Sep. 2006.

[15] T. Zhang, W. R. Eisenstadt, and R. M. Fox, "A novel 5 GHz RF power detector," in *Proc. IEEE Int. Symp. Circuits Syst.*, vol. 1. May 2004, pp. I-897–I-900.

[16] A. Vaneli-Corali *et al.*, "Satellite communications: Research trends and open issues," in *Proc. Int. Workshop Satellite Space Commun.*, Sep. 2007, pp. 71–75.